Robotica (2002) volume 20, pp. 251–260. © 2002 Cambridge University Press
DOI: 10.1017/S0263574702004198 Printed in the United Kingdom

Explicit force control for underwater vehicle-manipulator systems

Gianluca Antonelli,* Nilanjan Sarkar† and Stefano Chiaverini*

(Received in Final Form: October 29, 2001)

SUMMARY
In this paper two explicit force control schemes for underwater vehicle-manipulator systems are presented. The schemes take into account several factors such as uncertainty in the model knowledge, presence of hydrodynamic effects, kinematic redundancy of the system, and poor performance of vehicle's actuation system. The possible occurrence of loss of contact due to vehicle's movement during the task is also considered, and the adoption of an adaptive motion control scheme is investigated to take advantage of dynamic compensation. The proposed control schemes have extensively been tested in numerical simulation runs; the results obtained in a case study are reported to illustrate their performance.

KEYWORDS: Underwater robotics; Force control; Redundant robots; Underwater vehicle manipulator systems.

1. INTRODUCTION

We investigate the problem of an Underwater Vehicle-Manipulator System (UVMS) that interacts with the environment. An UVMS consists of an Autonomous Underwater Vehicle (AUV) and a robotic manipulator that is mounted on it. There are several difficulties that are associated with the control of an UVMS. First, it is usually difficult to have a precise model of the environment, which is both unstructured and time-varying. Second, UVMSs are complex systems that are difficult to model and control. The hydrodynamics of a multibody system is difficult to evaluate in realtime. The UVMS is a kinematically redundant system where the degrees of freedom associated with the AUV are less accurately controlled as compared to those of the manipulators. The dynamic coupling between the AUV and the manipulator makes it even more difficult to follow a desired trajectory and exert forces. All these factors make the problem of force control of UVMSs very challenging as well as a rewarding one.

Several force control schemes found in the literature deal with the frictionless contact between a manipulator and an elastically compliant environment (see reference [1, 2] for an overview). Stiffness and compliance control schemes[3] indirectly control the forces by assigning a stiffness behavior between the manipulator and the environment. Impedance control, on the other hand, allows the user to design a mechanical impedance of the system and control forces indirectly based on the designed impedance.[4]

In order to regulate the contact force we need what is called direct force control.[5] Closing an outer force feedback loop around the inner position/velocity feedback loop enables direct control of interaction force.[6] In interaction tasks, it is usually necessary to control both the end-effector position and the contact force simultaneously.[7] The hybrid force/position control scheme provides one such control action.[8] Force and motion are controlled in orthogonal directions in such control schemes. However, in order to achieve decoupling between force control and motion control, the task geometry must be known accurately. Since the underwater environment is poorly structured, hybrid control may not be a good choice for position/force control.

The parallel force/position control,[9] overcomes some of the problems associated with the hybrid control. In this case, position and force loops are closed in all task directions while structural properties of the controller ensure that properly assigned force reference value can be reached at the steady state. This control approach is robust to unplanned impacts. One drawback of the parallel control scheme is that the force and position loops are not decoupled and thus are subject to mutual disturbances during transients.

Force control with kinematic redundancy is still very much a research topic and so far they are related to land-based manipulators alone;[10–14] in this case, dynamic model parameters are well known and various dynamic compensation techniques can be used. Nevertheless, since UVMSs are poorly modeled, such techniques may not be appropriate for underwater task execution.

Regarding manipulation tasks for underwater robotic systems, in reference [15] the development of the project AMADEUS, a subsea hand carried by a manipulator and equipped with force and slip contact sensors, is described. Further detail can be found in reference [16] where the specific topic of two-degrees-of-freedom manipulator working in a cooperation task is investigated; the two manipulators are operated by a remote human operator. The force control scheme of each finger of the above hand is described in reference [17]. Reference [18] presents an impedance controller for UVMSs whose effectiveness has been proven in simulation. Reference [19] presents a hybrid force/position control of an underwater hydraulic

* Dipartimento di Automazione, Elettromagnetismo, Ingegneria dell'Informazione e Matematica Industriale, Università degli Studi di Cassino, Via G. Di Biasio 43, 03043 Cassino (FR) (Italy)
E-mail: {antonelli,chiaverini}@unicas.it
† Department of Mechanical Engineering, Vanderbilt University, Box 1592 Station B, Nashville, TN 37235 (USA), E-mail: nilanjan.sarkar@vanderbilt.edu

manipulator; experiments in 2 dofs are also provided with a Slingsby TA9. In reference [20] an external force control scheme for UVMSs is presented. It must be remarked that autonomous interaction tasks for UVMSs is a emerging research topic; very few papers treat the problem essentially from a theoretical/simulation point of view and the experiments have been conducted in safe and structured environments. Real UVMS' interaction tasks would benefit from the experience achieved from the practical problems encountered in remotely operated underwater vehicles carrying a manipulator, such as for example, Jason, of the Woods Hole Oceanographic Institution or Tiburon from the Monterey Bay Aquarium Research Institute. In detail, underwater sensors and actuators are characterized by poorer performances with respect to industrial applications in terms of bandwidth, noise and limit cycles.

In this paper, based on references [21–23] we present two force control schemes for UVMSs that overcome many of the above-mentioned difficulties associated with the underwater manipulation. These force control schemes exploit the system redundancy by using a task-priority based inverse kinematics algorithm.[24] This approach allows us to satisfy various secondary criteria while controlling the contact force. Both these force control schemes require separate motion control schemes which can be chosen to suit the objective without affecting the performance of the force control. The possible occurrence of loss of contact due to vehicle movement is also analyzed. The proposed control schemes have extensively been tested in numerical simulation runs; the results obtained in a case study are reported to illustrate their performance.

2. MODELLING

2.1. Kinematics

The vehicle is completely described by its position and orientation with respect to a reference frame that we will suppose earth-fixed and inertial. Let us define $\boldsymbol{\eta}=[\boldsymbol{\eta}_1^{\mathrm{T}} \ \boldsymbol{\eta}_2^{\mathrm{T}}]^{\mathrm{T}}$, where,$\boldsymbol{\eta}_1=[x\ y\ z]^T\in\mathbb{IR}^3$ is the vector of vehicle position coordinates in a earth-fixed reference frame and $\boldsymbol{\eta}_2=[\phi \ \ \theta \ \ \psi]^{\mathrm{T}}\in\mathbb{IR}^3$ is the vector of vehicle Euler-angle coordinates in a earth-fixed reference frame. The vectors $\dot{\boldsymbol{\eta}}_1$, $\dot{\boldsymbol{\eta}}_2$ are the corresponding time derivatives (expressed in the inertial frame).

Let us define $\boldsymbol{\nu}_1 \in \mathbb{IR}^3$ as the linear velocity of the vehicle-fixed frame with respect to the inertial frame expressed in the vehicle-fixed frame and $\boldsymbol{\nu}_2\in\mathbb{IR}^3$ as the angular velocity of the vehicle-fixed frame with respect to the inertial frame expressed in the vehicle-fixed frame.

Let $\boldsymbol{q}=[q_1 \ \ldots \ q_n]^T\in\mathbb{IR}^n$ be the vector of joint positions where n is the number of joints. The vector $\dot{\boldsymbol{q}}\in\mathbb{IR}^n$ is the corresponding time derivative. Let also define $\boldsymbol{\zeta}=[\boldsymbol{\nu}_1^{\mathrm{T}}\ \boldsymbol{\nu}_2^{\mathrm{T}}\ \dot{\boldsymbol{q}}^{\mathrm{T}}]^{\mathrm{T}}$.

The defined velocities are related via the following relation:

$$\boldsymbol{\zeta}=\begin{bmatrix}\boldsymbol{R}_I^B & \mathbf{O}_{3\times3} & \mathbf{O}_{3\times n}\\ \mathbf{O}_{3\times3} & \boldsymbol{J}_{k,o}(\boldsymbol{\eta}_2) & \mathbf{O}_{3\times n}\\ \mathbf{O}_{n\times3} & \mathbf{O}_{n\times3} & \mathbf{I}_{n,n}\end{bmatrix}\begin{bmatrix}\dot{\boldsymbol{\eta}}_1\\ \dot{\boldsymbol{\eta}}_2\\ \dot{\boldsymbol{q}}\end{bmatrix}=\boldsymbol{J}_k(\boldsymbol{\eta}_2)\begin{bmatrix}\dot{\boldsymbol{\eta}}_1\\ \dot{\boldsymbol{\eta}}_2\\ \dot{\boldsymbol{q}}\end{bmatrix} \quad (1)$$

where $\boldsymbol{R}_I^B$ is the rotation matrix expressing the transformation from the inertial frame to the vehicle-fixed frame; the matrix $\boldsymbol{J}_{k,o}$ can be expressed in terms of Euler angles as:

$$\boldsymbol{J}_{k,o}(\boldsymbol{\eta}_2)=\begin{bmatrix}1 & 0 & -s_\theta\\ 0 & c_\phi & c_\theta s_\phi\\ 0 & -s_\phi & c_\theta c_\phi\end{bmatrix} \quad (2)$$

where c_α and s_α are short notations for $\cos(\alpha)$ and $\sin(\alpha)$ respectively; $\boldsymbol{I}_{n,n}$ is the $(n\times n)$ identity matrix and $\boldsymbol{O}_{n_1,n_2}$ is the $(n_1\times n_2)$ null matrix.

Since the task is force/position control of the end effector frame, it is necessary to consider the position of the end effector in the inertial frame, $\boldsymbol{\eta}_{ee1}=[x_{ee}\ \ y_{ee}\ \ z_{ee}]^T\in\mathbb{IR}^3$. This is a function of the system configuration, i.e., $\boldsymbol{\eta}_{ee1}(\boldsymbol{\eta}, \boldsymbol{q})$. The vector $\dot{\boldsymbol{\eta}}_{\mathrm{ee1}}\in\mathbb{IR}^3$ is the corresponding time derivative.

Let us further define $\boldsymbol{\eta}_{ee2}\in\mathbb{IR}^3$ as the orientation of the end effector in the inertial frame expressed by Euler angles. Of course, also $\boldsymbol{\eta}_{ee2}$ is a function of the system configuration, i.e., $\boldsymbol{\eta}_{ee2}(\boldsymbol{\eta}, \boldsymbol{q})$. Again, the vector $\dot{\boldsymbol{\eta}}_{ee2}\in\mathbb{IR}^3$ is the corresponding time derivative.

The vectors $\dot{\boldsymbol{\eta}}_{ee1}$ and $\dot{\boldsymbol{\eta}}_{ee2}$ are related to the body-fixed velocities $\boldsymbol{\nu}_{ee}$ via relations analogous to Eq. (1), i.e.

$$\boldsymbol{\nu}_{ee1}=\boldsymbol{R}_I^n\dot{\boldsymbol{\eta}}_{ee1} \quad (3)$$

$$\boldsymbol{\nu}_{ee2}=\boldsymbol{J}_{k,o}(\boldsymbol{\eta}_{ee2})\dot{\boldsymbol{\eta}}_{ee2} \quad (4)$$

where $\boldsymbol{R}_I^n$ is the rotation matrix from the inertial to the end-effector frame (i.e., frame n) and $\boldsymbol{J}_{k,o}$ is the matrix defined in Eq. (2) where the end-effector Euler angles have to be considered.

The end-effector velocities (expressed in the inertial frame) are related to the body-fixed system velocity by a suitable Jacobian matrix:

$$\begin{bmatrix}\dot{\boldsymbol{\eta}}_{ee1}\\ \dot{\boldsymbol{\eta}}_{ee2}\end{bmatrix}=\begin{bmatrix}\boldsymbol{J}_{pos}(\boldsymbol{R}_B^I,\boldsymbol{q})\\ \boldsymbol{J}_{or}(\boldsymbol{R}_B^I,\boldsymbol{q})\end{bmatrix}\boldsymbol{\zeta}=\boldsymbol{J}_w(\boldsymbol{R}_B^I,\boldsymbol{q})\boldsymbol{\zeta} \quad (5)$$

2.2. Dynamics

The dynamic model of an UVMS can be written in the following compact form:[25,26]

$$\boldsymbol{M}(\boldsymbol{q})\dot{\boldsymbol{\zeta}}+\boldsymbol{C}(\boldsymbol{q},\boldsymbol{\zeta})\boldsymbol{\zeta}+\boldsymbol{D}(\boldsymbol{q},\boldsymbol{\zeta})\boldsymbol{\zeta}+\boldsymbol{g}(\boldsymbol{q},\boldsymbol{R}_B^I)=\boldsymbol{\tau} \quad (6)$$

where $\boldsymbol{M}(\boldsymbol{q})\in\mathbb{IR}^{(6+n)\times(6+n)}$ is the inertia matrix, $\boldsymbol{C}(\boldsymbol{q},\boldsymbol{\zeta})\boldsymbol{\zeta}\in\mathbb{IR}^{6+n}$ is the vector of Coriolis and centripetal terms, $\boldsymbol{D}(\boldsymbol{q},\boldsymbol{\zeta})\boldsymbol{\zeta}\in\mathbb{IR}^{6+n}$ is the vector of friction and hydrodynamic damping terms (e.g., drag, lift, and vortex shedding generalized forces), $\boldsymbol{g}(\boldsymbol{q},\ \boldsymbol{R}_I^B)\in\mathbb{IR}^{6+n}$ is the vector of gravitational and buoyant generalized forces, and $\boldsymbol{\tau}\in\mathbb{IR}^{6+n}$ is the vector of forces and moments acting on the vehicle as well as of the manipulator's joint torques.

Thrusters and control surfaces provide forces and moments on the vehicle according to a nonlinear relation. A simplified relationship can be expressed through the linear mapping[27]

$$\boldsymbol{\tau}=\boldsymbol{B}\boldsymbol{u}, \quad (7)$$

where $\boldsymbol{B}\in\mathbb{IR}^{(6+n)\times p}$, and $\boldsymbol{u}\in\mathbb{IR}^{p}$ is the vector of control inputs. In the remainder we will assume $p\geq(6+n)$ and $\boldsymbol{B}$ being full-rank.

It can be proven that:[26]

- the inertia matrix of the total system is positive definite and symmetric, i.e. $\boldsymbol{M}(\boldsymbol{q})=\boldsymbol{M}^{\mathrm{T}}(\boldsymbol{q})>\boldsymbol{O}$.
- the damping matrix is positive definite, i.e. $\boldsymbol{D}(\boldsymbol{q},\boldsymbol{\zeta})>\boldsymbol{O}$.
- the matrix $\boldsymbol{T}=\dot{\boldsymbol{M}}(\boldsymbol{q})-2\boldsymbol{C}(\boldsymbol{q},\boldsymbol{\zeta})$ is skew-symmetric, i.e. $\boldsymbol{\zeta}^{\mathrm{T}}\boldsymbol{T}\boldsymbol{\zeta}=0$.

Exploiting the linearity in the parameters,[28] equation (6) can be rewritten as:

$$\boldsymbol{Y}(\boldsymbol{R}_B^I,\boldsymbol{q},\boldsymbol{\zeta},\dot{\boldsymbol{\zeta}})\cdot\boldsymbol{\theta}=\boldsymbol{\tau}, \tag{8}$$

where $\boldsymbol{\theta}\in\mathbb{IR}^{w}$ is the vector of dynamic model parameters. For an underwater vehicle carrying a n-link manipulator the number of parameters of the whole system is $w=(n+1)\cdot h$, where h is the number of parameters for a single rigid body moving in a fluid. Notice that h usually is greater than 100.[27]

2.3. *Contact with the environment*

If the end effector of a robotic system is in contact with the environment the force/moment at the tip of the manipulator acts on the whole system according to the equation[29]

$$\boldsymbol{M}(\boldsymbol{q})\dot{\boldsymbol{\zeta}}+\boldsymbol{C}(\boldsymbol{q},\boldsymbol{\zeta})\boldsymbol{\zeta}+\boldsymbol{D}(\boldsymbol{q},\boldsymbol{\zeta})\boldsymbol{\zeta}+\boldsymbol{g}(\boldsymbol{q},\boldsymbol{R}_B^I)=\boldsymbol{\tau}+\boldsymbol{J}_w^{\mathrm{T}}(\boldsymbol{q},\boldsymbol{R}_B^I)\boldsymbol{h}, \tag{9}$$

where $\boldsymbol{h}=[\boldsymbol{f}^{\mathrm{T}}\quad\boldsymbol{\mu}^{\mathrm{T}}]^{\mathrm{T}}\in\mathbb{IR}^6$ are the force/moments at the end effector expressed in the inertial frame, $\boldsymbol{J}_w$ is the Jacobian defined in (5).

In the following we assume that only linear forces act on the end effector. Equation (9), thus, becomes

$$\boldsymbol{M}(\boldsymbol{q})\dot{\boldsymbol{\zeta}}+\boldsymbol{C}(\boldsymbol{q},\boldsymbol{\zeta})\boldsymbol{\zeta}+\boldsymbol{D}(\boldsymbol{q},\boldsymbol{\zeta})\boldsymbol{\zeta}+\boldsymbol{g}(\boldsymbol{q},\boldsymbol{R}_B^I)=\boldsymbol{\tau}+\boldsymbol{J}_{pos}^{T}(\boldsymbol{q},\boldsymbol{R}_B^I)\boldsymbol{f}. \tag{10}$$

Contact between the manipulator and the environment is usually difficult to model. In the following we will resort to the simple model constituted by a frictionless and elastically compliant plane. The force at the end effector is then related to the deformation of the environment by the following simplified model[9]

$$\boldsymbol{f}=\boldsymbol{K}(\boldsymbol{x}-\boldsymbol{x}_e), \tag{11}$$

where $\boldsymbol{x}$ is the position of the end effector expressed in the inertial frame, $\boldsymbol{x}_e$ characterizes the constant position of the unperturbed environment expressed in the inertial frame and

$$\boldsymbol{K}=k\boldsymbol{n}\boldsymbol{n}^{\mathrm{T}}, \tag{12}$$

with $k>0$, is the stiffness matrix $\boldsymbol{n}$ being the vector normal to the plane.[30] A sketch of the contact is shown in Fig. 1.

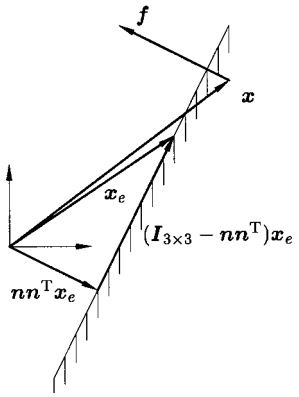

Fig. 1. Planar view of the chosen contact model.

In our case it is $\boldsymbol{x}=\boldsymbol{\eta}_{ee1}$; however, in the following the notation $\boldsymbol{x}$ will be maintained.

3. FORCE CONTROL SCHEME

The proposed force control schemes are inspired by the explicit force control presented in reference [23]. Two different versions of the scheme have been implemented based on different projections of the force error from the task space to the vehicle/joint space.

The first scheme is obtained by using the transpose of the Jacobian to project the force error from the task space directly to the control input space, i.e. force/moments for the vehicle and torques for the manipulator, leading to an evident physical interpretation.[21]任务空间到输入控制空间，物理意义明显

In the second scheme, instead, we project the force error from the task space to the body-fixed velocities.[22] This is done to avoid the need to directly access the control input; in many cases, in fact, a velocity controller is implemented on the manipulator, and control torques are not accessible.[23] 力误差从任务空间到体坐标系速度

3.1. *Force control scheme 1*

A sketch of the implemented scheme is provided in Fig. 2. In our case, the inverse kinematics is solved via a numerical algorithm based on velocity mapping to allow the handling of system redundancy efficiently (see Section 3.3). We can decompose the input torque into the sum of the torque output from the motion control and the torque output from the force control: $\boldsymbol{\tau}=\boldsymbol{\tau}^M+\boldsymbol{\tau}^F$. Following reference [21], the force control action $\boldsymbol{\tau}^F$ is computed as:

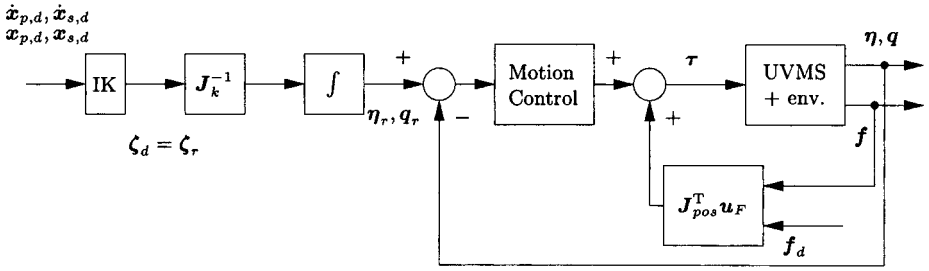

Fig. 2. Proposed force control scheme 1.

PID

$$\boldsymbol{\tau}^F = \boldsymbol{J}_{pos}^T \boldsymbol{u}_F = \boldsymbol{J}_{pos}^T \left(-\boldsymbol{f} + k_{f,p}\tilde{\boldsymbol{f}} - k_{f,v}\dot{\boldsymbol{f}} + k_{f,i}\int_0^t \tilde{\boldsymbol{f}}(\sigma)d\sigma \right), \quad (13)$$

where $k_{f,p}$, $k_{f,v}$, $k_{f,i}$ are scalar positive gains, and $\tilde{\boldsymbol{f}} = \boldsymbol{f}_d - \boldsymbol{f}$ is the force error. Equation (13), thus, is a force control action in the task space that is further projected, via the transpose of the Jacobian, on the vehicle/joint space. Notice that the units of the control gains must be properly defined so as to sum forces that, projected by the transpose of the Jacobian, lead to force/moment/torques coherently with the system's structure.

3.2. *Force control scheme 2*

A sketch of the implemented scheme is provided in Fig. 3. The force control action is composed of two loops; the action $-\boldsymbol{J}_{pos}^T \boldsymbol{f}$ is aimed at compensating the end-effector contact force (included in the block labeled "UVMS+env."). According to reference [22], the input of the motion control is a suitable integration of the velocity vector:

$$\boldsymbol{\zeta}_r = \boldsymbol{\zeta}_d + \boldsymbol{\zeta}_F = \boldsymbol{\zeta}_d + \boldsymbol{K}_{dim}\boldsymbol{J}_{pos}^T (k_{f,p}^* \tilde{\boldsymbol{f}} - k_{f,v}^* \dot{\boldsymbol{f}} + k_{f,i}^* \int_0^t \tilde{\boldsymbol{f}}(\sigma)d\sigma), \quad (14)$$

where $k_{f,p}^*$, $k_{f,v}^*$, $k_{i,i}^*$ are positive gains, and $\boldsymbol{\zeta}_d$ is the output of the inverse kinematics algorithm described in the next subsection. The units of the control gains are defined so as to sum forces that, projected by the transpose of the Jacobian, lead to force/moment/torques; the matrix $\boldsymbol{K}_{dim}$ =blockdiag $\{k_{dim1}\,\boldsymbol{I}_{3\times3}, k_{dim2}\,\boldsymbol{I}_{3\times3}, k_{dim3}\,\boldsymbol{I}_{n\times n}\}$, is defined in order to have the correct units such as to feed velocities to the motion controller (linear velocities, angular velocities and joint velocities).

3.3. *Inverse kinematics*

In this subsection the Inverse Kinematics (IK) algorithm, used for both controllers, is presented. Let m be the degrees-of-freedom of the mission task. The system dofs are $N=6+n$ where 6 are the dofs of the vehicle and n is the number of manipulator's joints.

When $N>m$ the system is redundant with respect to the given task and IK algorithms can be applied to exploit such redundancy. The IK algorithm implemented is based on the task-priority approach,[24,31] that allows to manage the natural redundancy of the system while avoiding the occurrence of algorithmic singularities.

Let define $\boldsymbol{x}_p$ as the primary task vector and $\boldsymbol{x}_s$ as the secondary task vector. The task priority inverse kinematics algorithm is based on the following update law

$$\boldsymbol{\zeta}_d = \boldsymbol{J}_p^{\#}[\dot{\boldsymbol{x}}_{p,d} + \boldsymbol{\Lambda}_p(\boldsymbol{x}_{p,d} - \boldsymbol{x}_p)] + (\boldsymbol{I} - \boldsymbol{J}_p^{\#}\boldsymbol{J}_p)\boldsymbol{J}_s^{\#}[\dot{\boldsymbol{x}}_{s,d} + \boldsymbol{\Lambda}_s(\boldsymbol{x}_{s,d} - \boldsymbol{x}_s)], \quad (15)$$

where $\boldsymbol{J}_p$ and $\boldsymbol{J}_s$ are the configuration-dependent primary and secondary task Jacobians respectively, the symbol # denotes a suitable matrix inversion (e.g. Moore-Penrose generalized inverse), $\boldsymbol{\Lambda}_p$ and $\boldsymbol{\Lambda}_s$ are positive definite matrices to be properly chosen.

Differently from the case of unconstrained motion tasks, when interaction with the environment occurs, the computation of $\boldsymbol{x}_p$ and $\boldsymbol{x}_s$ cannot be obtained directly from integration of the velocity output by the IK algorithm. In fact, the force control action may cause a significant difference between the reference and the actual motion variables. For this reason, the values of the actual motion variables must be used to compute $\boldsymbol{x}_p$ and $\boldsymbol{x}_s$ in Equation (15).

It is worth noting that UVMSs usually have many redundant degrees of freedom. For example, if a 6 dof manipulator is mounted on a vehicle, 12 dofs are available in total. In such cases, it is possible to define several tasks at different priority levels to be iteratively projected on the null space of the higher priority tasks.[32,33]

In the following we will assume $\boldsymbol{x}_p = \boldsymbol{x}$, i.e., the primary task is the end-effector force/position. The primary task Jacobian $\boldsymbol{J}_p$, thus, is the matrix $\boldsymbol{J}_{pos}$ defined in Equation (5).

3.4. *Motion control*

It must be remarked that the force control scheme 1 is not compatible with a motion control law with an integral action. In fact, since the position loop is closed around the force loop, this would cause rejection of the steady-state force control action. On the other hand, the force control scheme 2 is compatible with the use of an integral or an adaptive action in the motion control law. For this reason the first control scheme has been simulated using the control law described in Subsection 3.4.1 and the second control scheme has been simulated using the control law described in Subsection 3.4.2.

3.4.1. Sliding mode regulator for UVMSs. The control law is[34]

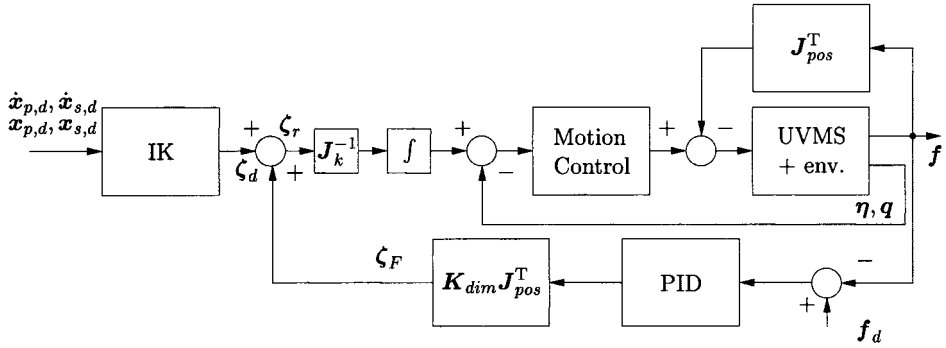

Fig. 3. Proposed force control scheme 2.

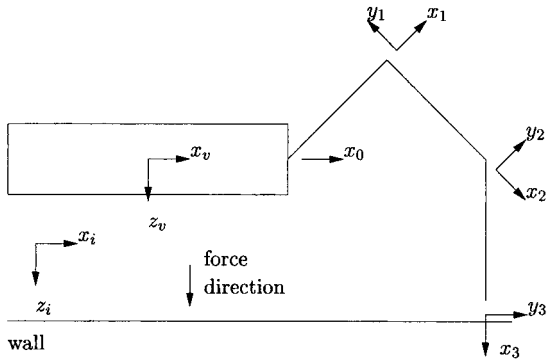

Fig. 4. Sketch of the system as seen from the xz vehicle-fixed plane.

$$\boldsymbol{\tau}^M = [\boldsymbol{K}_D \boldsymbol{s} + \hat{\boldsymbol{g}}(\boldsymbol{q}, \boldsymbol{R}_B^I) + \boldsymbol{K}\ \mathrm{sign}(\boldsymbol{s})], \tag{16}$$

where $\boldsymbol{K}_D$ is a positive definite gain matrix, $\hat{\boldsymbol{g}}(\boldsymbol{q}, \boldsymbol{R}_B^I)$ is the estimate of gravitational and buoyant forces, $\boldsymbol{K}$ is a positive definite matrix, and sign($\boldsymbol{x}$) is the vector function whose i-th component is

$$\mathrm{sign}(\boldsymbol{x})_i = \begin{cases} 1 & \text{if } x_i \geq 0 \\ -1 & \text{if } x_i < 0. \end{cases} \tag{17}$$

In equation (16), $\boldsymbol{s} \in \mathrm{I}\mathbb{R}^{6+n}$ is the sliding manifold defined as follows

$$\boldsymbol{s} = \begin{bmatrix} \tilde{\boldsymbol{\nu}}_1 \\ \tilde{\boldsymbol{\nu}}_2 \\ \dot{\tilde{\boldsymbol{q}}} \end{bmatrix} + \boldsymbol{\Lambda} \begin{bmatrix} \boldsymbol{R}_I^B \tilde{\boldsymbol{\eta}}_1 \\ \tilde{\boldsymbol{\varepsilon}} \\ \tilde{\boldsymbol{q}} \end{bmatrix} = \tilde{\boldsymbol{\zeta}} + \boldsymbol{y}, \tag{18}$$

with $\boldsymbol{\Lambda} > \boldsymbol{O}$, $\tilde{\boldsymbol{\nu}}_1 = \boldsymbol{\nu}_{1,r} - \boldsymbol{\nu}_1$, $\tilde{\boldsymbol{\nu}}_2 = \boldsymbol{\nu}_{2,r} - \boldsymbol{\nu}_2$, $\tilde{\boldsymbol{\eta}}_1 = [x_r - x\ y_r - y\ z_r - z]^{\mathrm{T}}$, $\tilde{\boldsymbol{q}} = \boldsymbol{q}_r - \boldsymbol{q}$ where the subscript r denotes reference values for the relevant variables, and $\tilde{\boldsymbol{\varepsilon}}$ is the vehicle attitude error expressed via quaternions.

If an estimate of the dynamic parameters in equation (6) is available, we might consider the control law

$$\boldsymbol{\tau}^M = [\boldsymbol{K}_D \boldsymbol{s} + \hat{\boldsymbol{g}} + \hat{\boldsymbol{M}}\dot{\boldsymbol{y}} + (\hat{\boldsymbol{C}} + \hat{\boldsymbol{D}})\boldsymbol{y} + \boldsymbol{K}\ \mathrm{sign}(\boldsymbol{s})]. \tag{19}$$

In view of practical implementation of eq. (16) the sign function is replaced by the sat function. sat($\boldsymbol{x}$, γ) is the vector function whose i-th component is

$$\mathrm{sat}(\boldsymbol{x}, \gamma)_i = \begin{cases} 1 & \text{if } x_i > \gamma \\ -1 & \text{if } x_i < -\gamma \\ \dfrac{x_i}{\gamma} & \text{otherwise.} \end{cases} \tag{20}$$

3.4.2. Virtual decomposition control for UVMS. Due to the poor knowledge of the system's dynamic parameters, implementation of an adaptive control law might be useful. However, because of the large value of w, an adaptive control law based on equation (8) would result in heavy computational burden. A numerically efficient approach to adaptive control of serial chain multi-body systems is the virtual decomposition method[35] which is based on a Newton-Euler (NE) formulation of the system dynamics. Its application to UVMSs has been proposed in reference [36].

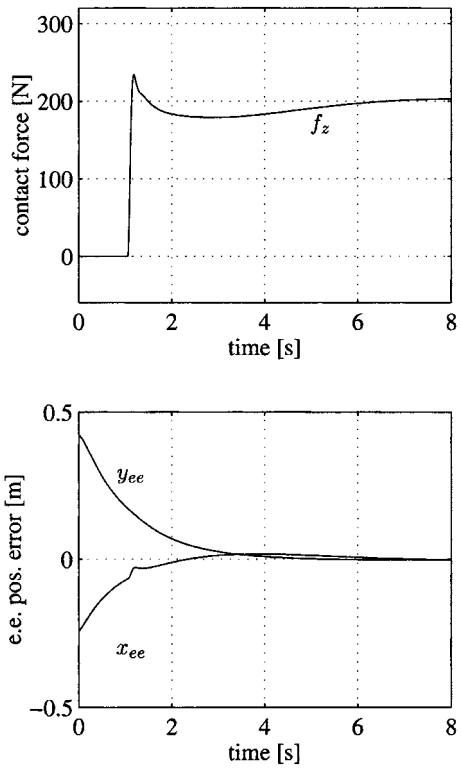

Fig. 5. Force control scheme 1. Top: Time history of the contact force. Bottom: Time history of the endeffector errors along the motion directions. The variables of the primary task are successfully controlled to their desired values.

The use of NE-based control laws makes it possible to compensate for the dynamics of complex structures such as UVMSs without requiring huge symbolic models. Moreover, the numerical complexity of the system only grows linearly for NE based models, while it does by a 4th order polynomial for Lagrange based models.

An UVMS can be regarded as an open chain of rigid bodies. Let us denote by the subscript i ($i=0, \ldots, n$) the generic rigid body of the system ($i=0$ denoting the vehicle).

From ($\boldsymbol{\zeta}_r$, $\boldsymbol{\eta}_r$, $\boldsymbol{q}_r$, it is possible to compute $\boldsymbol{p}_{d,i}(t)$, $Q_{d,i}(t)$, $\boldsymbol{\nu}_{d,i}^i(t)$ and $\dot{\boldsymbol{\nu}}_{d,i}^i(t)$ for $i=0, \ldots, n$ via forward kinematics of the manipulator. In the same way, from the sensor readings ($\boldsymbol{\zeta}$, $\boldsymbol{\eta}$, $\boldsymbol{q}$) it is possible to compute $\boldsymbol{p}_i(t)$, $Q_i(t)$ *and* $\boldsymbol{\nu}_i^i(t)$ for $i=0, \ldots, n$. Those are positions, quaternions, body-fixed velocities and accelerations of each rigid body. The superscript i indicates that the latter are expressed in their own frames.

It is then useful to consider the error vector $\boldsymbol{s}_i^i \in \mathrm{I}\mathbb{R}^6$ ($i=0 \ldots n$):

$$\boldsymbol{s}_i^i = \boldsymbol{\nu}_{d,i}^i - \boldsymbol{\nu}_i^i + \boldsymbol{\Lambda}_i \boldsymbol{e}_i, \tag{21}$$

where

$$\boldsymbol{e}_i = \begin{bmatrix} \boldsymbol{R}_i^{I\mathrm{T}}(\boldsymbol{p}_{d,i} - \boldsymbol{p}_i) \\ \tilde{\boldsymbol{\varepsilon}}_i \end{bmatrix} \tag{22}$$

is the (6×1) vector of position and orientation errors for each body, and the matrix gain $\boldsymbol{\Lambda}_i$ is defined as

$$\boldsymbol{\Lambda}_i = \text{blockdiag}\{\lambda_{p,i}\boldsymbol{I}_{3\times 3}, \lambda_{o,i}\boldsymbol{I}_{3\times 3}\}, \quad (23)$$

with $\lambda_{p,i}>0$, $\lambda_{o,i}>0$.

The end-effector frame is attached to the last link (i.e. the n-th rigid body) and the required force/moment acting on it is given by reference [35]:

$$\boldsymbol{f}^{\,n}_{r,n} = \boldsymbol{Y}'(\boldsymbol{R}^I_n, \boldsymbol{v}^n_n, \dot{\boldsymbol{v}}^n_{d,n} + \boldsymbol{\Lambda}_n\dot{\boldsymbol{e}}_n)\hat{\boldsymbol{\theta}}_n + \boldsymbol{K}_{v,n}\boldsymbol{s}^n_n + \boldsymbol{K}_{p,n}\boldsymbol{e}_n, \quad (24)$$

where $\boldsymbol{Y}' \in \mathbb{IR}^{6\times h}$ iSs the rigid-body regressor matrix, $\boldsymbol{K}_{v,n}>\boldsymbol{O}$, and $\boldsymbol{K}_{p,n}=\text{blockdiag}\{k_p\boldsymbol{I}_{3\times 3}, k_o\boldsymbol{I}_{3\times 3}\}$, with $k_p>0$ and $k_o>0$. The dynamic parameters estimate $\hat{\boldsymbol{\theta}}_n$ is updated as follows

$$\dot{\boldsymbol{\theta}}_n = \boldsymbol{K}^{-1}_{\theta,n}\boldsymbol{Y}'^{\mathrm{T}}(\boldsymbol{R}^I_n, \boldsymbol{v}^n_n, \dot{\boldsymbol{v}}^n_{d,n} + \boldsymbol{\Lambda}_n\boldsymbol{e}_n)\,\boldsymbol{s}^n_n \quad (25)$$

with $\boldsymbol{K}_{\theta,n}>\boldsymbol{O}$.

For the other n rigid bodies (including the vehicle) the required force has an analogous structure, except for the absence of the term $\boldsymbol{K}_{p,i}\boldsymbol{e}_i$; thus, for $i=0,\ldots,n-1$ the required force and parameters estimate is given by

$$\boldsymbol{f}^i_{r,i} = \boldsymbol{Y}'(\boldsymbol{R}^I_i, \boldsymbol{v}^i_i, \dot{\boldsymbol{v}}^i_{d,i} + \boldsymbol{\Lambda}_i\dot{\boldsymbol{e}}_i)\hat{\boldsymbol{\theta}}_i + \boldsymbol{K}_{v,i}\boldsymbol{s}^i_i \quad (26)$$

$$\dot{\hat{\boldsymbol{\theta}}}_i = \boldsymbol{K}^{-1}_{\theta,i}\boldsymbol{Y}'^{\mathrm{T}}(\boldsymbol{R}^I_i, \boldsymbol{v}^i_i, \dot{\boldsymbol{v}}^i_{d,i} + \boldsymbol{\Lambda}_i\dot{\boldsymbol{e}}_i)\boldsymbol{s}^i_i \quad (27)$$

with $\boldsymbol{K}_{v,i}>\boldsymbol{O}$ and $\boldsymbol{K}_{\boldsymbol{\theta},i}>\boldsymbol{O}$.

Notice that the regressor $\boldsymbol{Y}'$ used in the control laws (24)–(27) is relative to a single rigid body moving in a fluid, whereas the regressor $\boldsymbol{Y}$ in equation (8) is relative to the whole UVMS. Moreover, the regressor $\boldsymbol{Y}'$ has the same structure for all the rigid bodies leading to a simple software realization.

The control torque at the i-th manipulator's joint is the sum of the torque needed to achieve the required force on the i-th link and a joint velocity feedback term, i.e.

$$\tau_i = \boldsymbol{z}^{iT}_{i-1}(\boldsymbol{f}^i_{r,i} + \boldsymbol{U}^i_{i+1}\boldsymbol{f}^{i+1}_{r,i+1}) + k_{vq,i}\dot{\tilde{q}}_i \quad (28)$$

where $k_{vq,i}>0$, $\dot{\tilde{q}}_i = \dot{q}_{r,i} - \dot{q}_i$, and the matrix $\boldsymbol{U}^i_{i+1} \in \mathbb{IR}(6\times 6)$ is defined as

$$\boldsymbol{U}^i_{i+1} = \begin{bmatrix} \boldsymbol{R}^i_{i+1} & \boldsymbol{O}_{3\times 3} \\ \boldsymbol{S}(\boldsymbol{r}^i_{i,i+1})\boldsymbol{R}^i_{i+1} & \boldsymbol{R}^i_{i+1} \end{bmatrix} \quad (29)$$

being $\boldsymbol{S}(\cdot)$ the matrix operator needed to perform the cross product.

Finally, the generalized force for the vehicle needed to achieve the corresponding required force is computed as

$$\boldsymbol{f}^{\,0}_0 = \boldsymbol{f}^{\,0}_{r,0} + \boldsymbol{U}^0_1\boldsymbol{f}^1_{r,1}. \quad (30)$$

To summarize, the steps necessary to implement the motion control algorithm are the following:

(i) from $\boldsymbol{\zeta}_r, \boldsymbol{\eta}_r, \boldsymbol{q}_r$ compute $\boldsymbol{p}_{d,i}$, $Q_{d,i}$, $\boldsymbol{v}^i_{d,i}$ and $\dot{\boldsymbol{v}}^i_{d,i}(t)$ for $i=0,\ldots,n$ by forward kinematics;
(ii) from $\boldsymbol{\zeta}, \boldsymbol{\eta}, \boldsymbol{q}$ compute $\boldsymbol{p}_i$, Q_i, and $\boldsymbol{v}^i_i$ for $i=0,\ldots,n$ by forward kinematics;
(iii) compute $\boldsymbol{f}^{\,i}_{r,i}$ and $\dot{\hat{\boldsymbol{\theta}}}_i$ for $i=1\ldots n$ by equations (21)–(27);
(iv) compute τ_i for $i=n,\ldots,1$ by equation (28);
(v) compute $\boldsymbol{f}^{\,0}_0$ by equation (30).

3.5. Robustness

In the following, the robustness of the schemes to react against unexpected impacts or errors in planning desired force/position directions is discussed.

The proposed scheme shows the same feature as the parallel control; in fact, the use of the integral action in the force controller gives a higher priority to the force error with respect to the position error. In detail, let define a base frame for the task space. Together with the vector $\boldsymbol{n}$ already defined, let introduce two vectors $\boldsymbol{m}$ and $\boldsymbol{l}$ such that an orthonormal frame is completed; these two vectors define the motion directions. Since $\boldsymbol{f}_d \in \mathcal{R}(\boldsymbol{K})$ the following relationships hold:

$$\boldsymbol{m}^{\mathrm{T}}\boldsymbol{f}_d = 0,$$
$$\boldsymbol{l}^{\mathrm{T}}\boldsymbol{f}_d = 0$$

meaning that a null desired force is commanded along the motion directions.

Let consider the first control scheme. If the motion control does not have an integral action such as a, e.g., PD+compensation action, the occurrence of an unexpected impact is safely handled by the control scheme. Consider an unexpected impact along $\boldsymbol{m}$; the force loop will charge the integral action in order to obtain the desired null contact force in that direction. However, the output of the motion control is seen as a constant disturbance at steady state and is rejected as well. In the direction $\boldsymbol{m}$, thus, a position error is experienced to allow achieving a null contact force.

For the second control scheme there is the possibility to use an adaptive or integral action also in the motion control. A contact in the $\boldsymbol{m}$ direction would be projected as a velocity reference in the vehicle/joint space; at steady state, with a null contact force along $\boldsymbol{m}$, the reference position, obtained by integration of the reference velocity, takes into account the modified path in order to avoid a force along $\boldsymbol{m}$ (see Figure 3). This reference position can be tracked with the desired motion control, thus achieving the possibility to use adaptive actions.

If $\boldsymbol{f}_d \notin \mathcal{R}(\boldsymbol{K})$, i.e. the direction of $\boldsymbol{f}_d$ is not parallel to $\boldsymbol{n}$, the controller is commanded to interact with the environment in directions along which no reaction force exists. In that case, a drift motion in that direction is experienced.

3.6. Loss of contact

In case of loss of contact the force error is projected on either the generalized force space for the first control law or the vehicle/joint velocity space for the second control law with undesired effects. We handle this problem by resetting the integrator in the force controller when the force sensor does not read any force value in the desired contact direction; accordingly, equation (15) is modified as follows:

$$\boldsymbol{\zeta}_d = \boldsymbol{J}^{\#}_p\{\boldsymbol{H}[\dot{\boldsymbol{x}}_{p,d} + \boldsymbol{\Lambda}_p(\boldsymbol{x}_{p,d} - \boldsymbol{x}_p)] + (\boldsymbol{I} - \boldsymbol{H})\dot{\boldsymbol{x}}_l\}$$
$$+ (\boldsymbol{I} - \boldsymbol{J}_p\boldsymbol{J}^{\#}_p)\boldsymbol{J}^{\#}_s[\dot{\boldsymbol{x}}_{s,d} + \boldsymbol{\Lambda}_s(\boldsymbol{x}_{s,d} - \boldsymbol{x}_s)] \quad (31)$$

where $\boldsymbol{H} \in \mathbb{IR}^{m\times m}$ is a diagonal matrix with ones for the motion directions and zeros for the force directions, and $\dot{\boldsymbol{x}}_l$ is a desired velocity at which the end effector can safely impact the environment.

The matrix $\boldsymbol{H}$ can be viewed as the selection matrix of a hybrid control scheme. Remarkably, this matrix is used only when there is *no contact* at the end effector; therefore, the robustness properties discussed above still hold. Notice that,

the use of $\boldsymbol{H}$ only requires knowledge of the normal direction of the contact surface.

3.7. Implementation issues

The practical implementation of the proposed force control schemes might benefit from some considerations:

- Force control task requires accurate positioning of the end effector. On the other hand, the vehicle, i.e. the base of the manipulator, is characterized by large positioning errors. Thus, in equation (15) it could be appropriate to decompose the desired end-effector velocities in a way to involve the manipulator alone in the fulfilment of the primary task. If we define as $\boldsymbol{J}_{p,man}(\boldsymbol{\eta}_2, \boldsymbol{q})$ the Jacobian of the manipulator, we can rewrite equation (15) as

$$\boldsymbol{\zeta}_d = \begin{bmatrix} \boldsymbol{0}_{6\times 1} \\ \boldsymbol{J}^{\#}_{p,man}[\dot{\boldsymbol{x}}_{p,d} + \boldsymbol{\Lambda}_p(\boldsymbol{x}_{p,d} - \boldsymbol{x}_p)] \end{bmatrix} + (\boldsymbol{I} - \boldsymbol{J}^{\#}_p \boldsymbol{J}_p)\boldsymbol{J}^{\#}_s[\dot{\boldsymbol{x}}_{s,d} + \boldsymbol{\Lambda}_s(\boldsymbol{x}_{s,d} - \boldsymbol{x}_s)]. \quad (32)$$

  Notice that the same properties of equation (15) applies also for equation (32). A physical interpretation is the following: we *ask* the manipulator to fulfill the primary task taking into account the movement of its base. At the same time we fulfil secondary tasks, with less strict requirements, with the whole system (e.g., the vehicle must move when the manipulator is working on the boundaries of its workspace).
- To decrease power consumption it is possible to implement IK algorithms with bounded reference values for the secondary tasks. Using some smooth functions, or fuzzy techniques,[32] it is possible to activate the secondary tasks only when the relevant variables are out of a desired range. For the roll and pitch vehicle's angles, for example, it is sufficient to implement an algorithm that keeps them in a range of, e.g., $\pm 10°$.
- The regressor of an underwater vehicle does not depend on the actual position of the vehicle (see equation (6)). If a model-based adaptive control law is applied, then, it cannot compensate for disturbances or model mismatching that affect the vehicle position. For example, if a linear constant ocean current acts on the vehicle, at steady state a non-null position error is experienced. A suitable integral action might be added to the control law to overcome this problem.
- The mathematical model of a single rigid body moving in a fluid is very complex.[27] To reduce the computational burden, since the force control task is usually performed while the vehicle is in hovering, i.e. at small velocities, we can implement the adaptive control law only with respect to the parameters that may cause steady state errors. In this case, therefore, only the parameters related to the restoring forces and to the ocean current are included in $\hat{\boldsymbol{\theta}}_i$.
- Force/moment sensor readings are usually corrupted by noise. The use of a derivative action in the control law, thus, can be difficult to implement. With the assumption of a frictionless and elastically compliant contact plane we observe a linear relation between $\dot{\boldsymbol{f}}$ and $\dot{\boldsymbol{x}}$. The force derivative action can then be substituted by a term proportional to $\dot{\boldsymbol{x}}$. The latter will be computed by differential kinematics from $\boldsymbol{\zeta}$ that is usually available from direct sensor readings or from the position readings via a numerical filter.

4. CASE STUDY

To test the effectiveness of the proposed force control schemes several numerical simulations have been run under the MATLAB 5.2/SIMULINK 2.0 environment. The controllers have been implemented in discrete time with a sampling frequency of 200 Hz. The environmental stiffness is $k = 10^4$ N/m.

The simulated UVMS has 9 dofs, 6 dofs of the vehicle plus a 3-link manipulator mounted on it.[37] The vehicle is a box of dimensions $(2 \times 1 \times 0.5)$ m; the vehicle-fixed frame is located in the geometrical center of the body. The manipulator is a 3-link planar manipulator with rotational joints. The overall system simulated has more than 50 dynamic parameters. Figure 4 shows a sketch of the system, seen from the vehicle's xz plane, in the configuration

$$\boldsymbol{\eta} = [0 \;\; 0 \;\; 0 \;\; 0 \;\; 0 \;\; 0]^{\mathrm{T}} \quad [\mathrm{m, deg}]$$
$$\boldsymbol{q} = [45 \;\; -90 \;\; -45]^{\mathrm{T}} \quad [\mathrm{deg}] \quad (33)$$

corresponding to the end-effector position $\boldsymbol{\eta}_{ee1} = [2.41 \;\; 0 \;\; 1]^{\mathrm{T}}$ m.

A case study has been considered aimed at the following objectives: as primary task, to perfom force/motion control

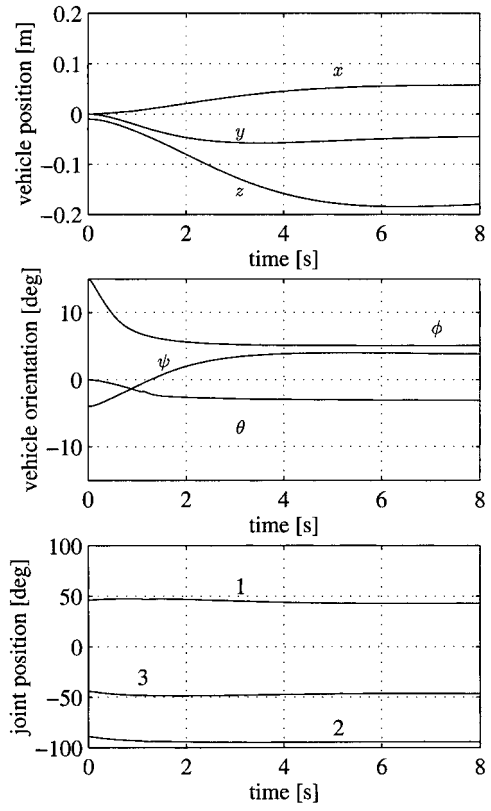

Fig. 6. Force control scheme 1. Top: Time history of the vehicle's position. Center: Time history of the vehicle's orientation. Bottom: Time history of the joint positions. By exploiting the system redundancy, the vehicle orientation is kept in a desired range. Moreover, the primary and secondary tasks are performed despite the poor vehicle controller.

of the end-effector (exert a force of 200 N along z_i, moving the end effector from 2.41 m to 2.21 m along x_i, while keeping y_i at 0 m); as secondary task, to guarantee vehicle's roll and pitch angles being kept in the range $\pm 10°$; as tertiary task, to guarantee the manipulator's manipulability being kept in a safe range. In detail, the 3 task variables are:

$$\boldsymbol{x}_p = \boldsymbol{x} \quad \boldsymbol{x}_s = [\phi \quad \theta]^{\mathrm{T}} \quad x_t = q_2, \tag{34}$$

where x_t expresses the third task; in fact, since the manipulator has a 3-link planar structure, a measure of its manipulability is simply given by q_2, where $q_2 = 0$ corresponds to a kinematic singularity.

We suppose that the system starts the mission in the non-dexterous configuration

$$\begin{aligned} \boldsymbol{\eta} &= [0 \;\; 0 \;\; -0.01 \;\; 15 \;\; 0 \;\; -4]^{\mathrm{T}} \;\; [\mathrm{m, deg}] \\ \boldsymbol{q} &= [46 \;\; -89 \;\; -44]^{\mathrm{T}} \qquad\quad [\mathrm{deg}] \end{aligned} \tag{35}$$

corresponding to the end-effector position $\boldsymbol{\eta}_{ee1} = [2.45 \;\; -0.42 \;\; 0.91]^{\mathrm{T}}$ m. In the initial configuration, thus, the system is not in contact with the environment.

A weighted pseudoinverse has been used to compute $\boldsymbol{J}^{\#}$ with weigh matrix $\boldsymbol{W} = \mathrm{blockdiag}\{10 \cdot \boldsymbol{I}_{6\times 6}, 1 \cdot \boldsymbol{I}_{3\times 3}\}$. To simulate an imperfect hovering of the vehicle we have implemented the control law with *lower* gains for the vehicle; the performance of the simulated vehicle, thus, has an error that is of the same magnitude of a real vehicle in hovering.

To accomplish the above task, first the force control scheme 1 is used together with the sliding mode motion control law described in Subsection 3.4.1; notice that non-perfect gravity and buoyancy compensation has been assumed. The control gains used in the force loop are the following: $k_{f,p} = 1.2$, $k_{f,v} = 0.1$, $k_{f,i} = 1.25$. Figure 5 reports the contact force and the end-effector error components obtained. Since the desired final position is given as a set-point, the initial end-effector position errors are big. However, they are quickly recovered. In Fig. 6, the position and orientation components of the vehicle and the joint positions are shown; it can be recognized that, despite the large starting value, the roll angle is kept in the desired range. Also, despite the desired null motion of the vehicle, the imperfect restoring compensation and the coupling with the manipulator cause a large movement that, however, does not affect significantly the tasks due to the proper motion distribution achieved with the applied kinematic control.

To take advantage of dynamic compensation actions, the force control scheme 2 is used to accomplish the same task as above together with the singularity-free adaptive control presented in Subsection 3.4.2; notice that only the restoring force terms have been considered to be compensated and a constant unknown error, bounded to $\pm 10\%$, of these parameters has been assumed. There are 4 parameters for

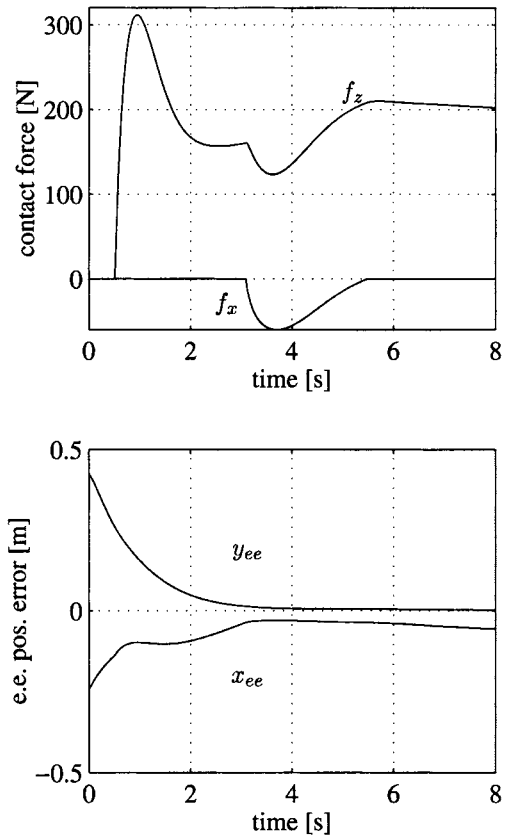

Fig. 7. Force control scheme 2. Top: Time history of the contact force in case of unexpected impact along x_i. Bottom: Time history of the end-effector errors along the motion directions. It can be observed that the control scheme automatically relaxes the motion constraint when the unexpected impact arises along x_i; thus, a position error is experienced.

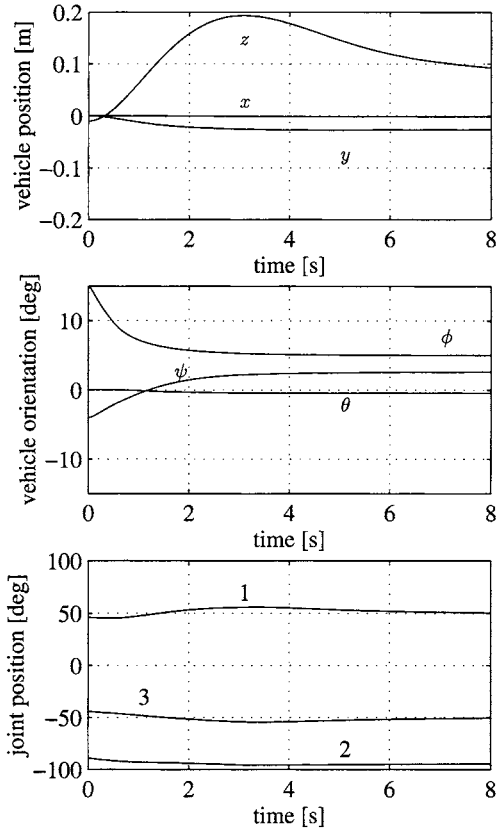

Fig. 8. Force control scheme 2. Top: Time history of the vehicle's position. Center: Time history of the vehicle's orientation. Bottom: Time history of the joint positions. Notice that the use of an adaptive action allows the vehicle to recover the initial position, however this is obtained with a *slow* time constant while the force task is performed mainly with the manipulator.

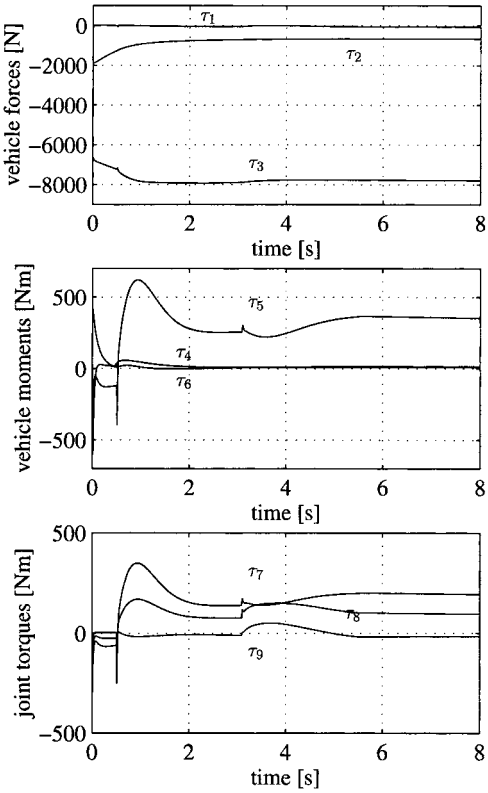

Fig. 9. Force control scheme 2. Top: Time history of the vehicle's linear forces. Center: Time history of the vehicle's moments. Bottom: Time history of the joint torques. The impact effects can be easily recognized.

each rigid body of the UVMS, giving 16 parameters in total. The control gains used in the force loop are the follows: $k^*_{f,p}$=4 10^{-4}, $k^*_{f,v}$=1 10^{-5}, $k^*_{f,i}$=4.8 10^{-4}. Moreover, during the task execution an unexpected impact occurs along x_i.

In Fig. 7, the contact force and the end-effector error components are shown. It can be recognized that the unexpected impact, occurring at about 3 s, is safely handled: a transient force component along x_i is experienced; nevertheless, at the steady state the desired force is achieved with null error. This, of course, causes a steady state error in the x_i direction.

In Fig. 8, the vehicle's position and orientation components and the joint positions are shown. It can be recognized that the vehicle moves by about 10 cm; nevertheless, the manipulator still performs the primary task accurately. Moreover, the large initial roll angle is recovered by exploiting the system redundancy since this task does not conflict with the higher priority task.

Finally, in Fig. 9 the control input for the last simulation is shown. The two impacts can be easily observed; moreover, the control inputs are smooth.

5. CONCLUSIONS

In this paper two explicit force control schemes for underwater vehicle-manipulator systems have been presented which are suited to the execution of autonomous underwater missions. Several design constraints are taken into account, namely, modelling uncertainties, presence of hydrodynamic effects, kinematic redundancy of the system, and difficulty in vehicle hovering. The possible occurrence of loss of contact due to vehicle movement during the task has also been considered.

In the force control scheme 1 the force error directly modifies the force/moments/torques acting on the UVMS, leading to an evident physical interpretation. In the force control scheme 2, instead, the force error builds a correction term acting on the body-fixed velocity references which fed the available motion control system of the UVMS.

The two proposed control schemes have been tested in numerical simulation case studies and their performance is analyzed. Overall, the force control scheme 2 seems to be preferable with respect to the force control scheme 1 for two reasons: First, it allows the adoption of adaptive motion control laws, thus making possible dynamic compensation actions. Second, it naturally embeds the standard motion control of the UVMS, since it acts at the reference motion variables level.

ACKNOWLEDGEMENTS

This work was funded in part by the following grants: NSF (BES97–01614) and ONR (N00014–97–10961). The views expressed herein are those of the authors and do not necessarily reflect the views of funding agencies.

References

1. B. Siciliano and L. Villani, *Robot Force Control* (Kluwer Academic Publishers, Boston, MA, 1999).
2. D. E. Whitney, "Historical Perspective and State of the Art in Robot Force Control," *Int. J. Robotics Research* **6**(1), 3–14 (1987).
3. J. K. Salisbury, "Active Stiffness Control of a Manipulator in Cartesian Coordinates," *Proc. 19th IEEE Conf. on Decision and Control*, Albuquerque, NM (1980) pp. 95–100.
4. N. Hogan, "Impedance Control: An Approach to Manipulation," *(Parts I-III) Trans. ASME J. of Dynamic Systems, Measurement, and Control* (1985), **Vol. 107**, pp. 1–24.
5. D. E. Whitney, "Force Feedback Control of Manipulators Fine Motions," *Trans. ASME J. of Dynamic Systems, Measurement, and Control* **99**, 91–97 (1977).
6. J. De Schutter and H. Van Brussel, "Compliant Robot Motion II. A Control Approach Based on External Control Loops," *Int. J. Robotics Research* **7**(4), 18–33 (1988).
7. M. T. Mason, "Compliance and Force Control for Computer Controlled Manipulators," *IEEE Trans. on Systems, Man, and Cybernetics* **11**, 418–432 (1981).
8. M. H. Raibert and J. J. Craig, "Hybrid Position/Force Control of Manipulators," *Trans. ASME J. of Dynamic Systems, Measurement, and Control* **102**, 126–133 (1981).
9. S. Chiaverini and L. Sciavicco, "The Parallel Approach to Force/Position Control of Robotic Manipulators," *IEEE Trans. on Robotics and Automation* **9**, 361–373 (1993).
10. O. Khatib, "A Unified Approach for Motion and Force Control of Robot Manipulators: The Operational Space Formulation," *IEEE J. of Robotics and Automation* **3**, 43–53 (1987).
11. C. Natale, B. Siciliano and L. Villani, "Spatial Impedance Control of Redundant Manipulators," *Proc. IEEE Int. Conf. on Robotics and Automation*, Detroit, (1999) pp. 1788–1793.
12. B. Nemec, "Force Control of Redundant Robots," *Prep. 5th IFAC Symp. on Robot Control, Nante* (1997) pp. 215–220.
13. Y. Oh, W. K. Chung, Y. Youm and I. H. Suh, "Motion/Force Decomposition of Redundant Manipulator and Its Application to Hybrid Impedance Control," *Proc. IEEE Int. Conf. on Robotics and Automation*, Leuven, Belgium (1998) pp. 1441–1446.

14. Z. Peng and N. Adachi, "Compliant Motion Control of Kinematically Redundant Manipulators," *IEEE Trans. on Robotics and Automation* **9**, 831–837 (1993).
15. D. M. Lane et al., "AMADEUS: Advanced MAnipulation for DEep Underwater Sampling," *IEEE Robotics and Automation Magazine* **4**, 34–45 (1997).
16. D. Angeletti, G. Bruzzone, M. Caccia, G. Cannata, G. Casalino, S. Reto and G. Verrugio, "AMADEUS: Dual-Arm Workcell for Co-ordinated and Dexterous Manipulation," *Oceans' 98*, Vancouver, Canada (1998) pp. 947–952.
17. D. J. O'Brien and D. M. Lane "3D Force Control System Design for a Hydraulic Parallel Bellows Continuum Actuator," *Proc. IEEE Int. Conf. on Robotics and Automation*, Seoul, Korea (2001) pp. 2375–2380.
18. Y. Cui, T. Podder and N. Sarkar, "Impedance Control of Underwater Vehicle-Manipulator Systems (UVMS)," *Proc. 1999 IEEE/RSJ Int. Conf. on Intelligent Robots and Systems* (1997) pp. 148–153.
19. M. W. Dunningan, D. M. Lane, A. C. Clegg and I. Edwards, "Hybrid Position/Force Control of a Hydraulic Underwater Manipulator," *IEE Proc. Control Theory Appl*, (1996) **Vol. 143**, pp. 145–151.
20. G. Antonelli, N. Sarkar and S. Chiaverini, "External Force Control for Underwater Vehicle-Manipulator Systems," *Proc. 38th IEEE Conference on Decision and Control*, Phoenix, AZ (1999) pp. 2975–2980.
21. G. Antonelli, S. Chiaverini and N. Sarkar, "An Explicit Force Control Scheme for Underwater Vehicle-Manipulator Systems," *Proc. IEEE/RSJ Int. Conf. on Intelligent Robots and Systems*, Kyongju, Korea (1999) pp. 136–141.
22. G. Antonelli, S. Chiaverin and N. Sarkar, "Explicit Force Control for Underwater Vehicle-Manipulator Systems with Adaptive Motion Control Law," *Proc. IEEE Hong Kong Symp. on Robotics and Control*, Hong Kong, PRC (1999) pp. 361–366.
23. G. Ferretti, G. Magnani and P. Rocco, "Toward the Implementation of Hybrid Position/Force Control in Industrial Robots," *IEEE Trans. on Robotics and Automation* **16**, 838–845 (1997).
24. S. Chiaverini, "Singularity-Robust Task-Priority Redundancy Resolution for Real-Time Kinematic Control of Robot Manipulators," *IEEE Trans. on Robotics and Automation* **13**, 398–410 (1997).
25. N. Sarkar and T. K. Podder, "Motion Coordination of Underwater VehicleManipulator Systems Subject to Drag Optimization," *Proc. IEEE Int. Conf on Robotics and Automation*, Detroit, MI (1999) pp. 387–392.
26. I. Schjølberg and T. I. Fossen, "Modelling and Control of Underwater Vehicle-Manipulator Systems," *Proc. 3rd Conf. on Marine Craft Manoeuvring and Control*, Southampton, UK (1994) pp. 45–47.
27. T. Fossen, *Guidance and Control of Ocean Vehicles* (John Wiley & Sons, Chichester, UK, 1994).
28. T. Fossen, "Adaptive Macro-Micro Control of Nonlinear Underwater Robotic Systems," *Proc. 5th Int. Conf. on Advanced Robotics*, Pisa, Italy (1991) pp. 1569–1572.
29. L. Sciavicco and B. Siciliano, *Modeling and Control of Robot Manipulators* (Springer-Verlag, London, UK, 2000).
30. J. Loncaric, "Normal Forms of Stiffness and Compliance Matrices," *IEEE J. of Robotics and Automation* **3**, 567–572 (1987).
31. G. Antonelli and S. Chiaverini, "Task-Priority Redundancy Resolution for Underwater Vehicle-Manipulator Systems," *Proc. IEEE Int. Conf. on Robotics and Automation*, Leuven, Belgium (1998) pp. 768–773.
32. G. Antonelli and S. Chiaverini, "A Fuzzy Approach to Redundancy Resolution for Underwater Vehicle-Manipulator Systems," *5th IFAC Conference on Manoeuvring and Control of Marine Craft*, Aalborg, Denmark (2000).
33. B. Siciliano and J.-J.E. Slotine, "A General Framework for Managing Multiple Tasks in Highly Redundant Robotic Systems," *Proc. 5th Int. Conf. on Advanced Robotics*, Pisa, Italy (l991) pp. 1211–1216.
34. G. Antonelli and S. Chiaverini, "Singularity-Free Regulation of Underwater Vehicle-Manipulator Systems," *Proc. American Control Conference*, Philadelphia, PA (1998) pp. 399–403.
35. W. H. Zhu, Y. G. Xi, Z. J. Zhong, Z. Bie and J. De Schutter, "Virtual Decomposition Based Control for Generalized High Dimensional Robotic Systems with Complicated Structure," *IEEE Trans. on Robotics and Automation* **13**, 411–436 (1997).
36. G. Antonelli, F. Caccavale and S. Chiaverini, "A Modular Scheme for Adaptive Control of Underwater Vehicle-Manipulator Systems," *Proc. American Control Conference*, San Diego, CA (1999) pp. 3008–3012.
37. T. K. Podder, "Dynamic and Control of Kinematically Redundant Underwater Vehicle-Manipulator Systems," *Autonomous Systems Laboratory Technical Report, vol. ASL 98-01* (University of Hawaii, Honolulu, HI, 1998).